JOURNAL OF THE MECHANICAL BEHAVIOR OF BIOMEDICAL MATERIALS 29 (2014) 582–593

Available online at www.sciencedirect.com

ScienceDirect

www.elsevier.com/locate/jmbbm

Research Paper

On a new model for inhomogeneous volume growth of elastic bodies

Markus Böl*, **Antonio Bolea Albero**

Institute of Solid Mechanics, Technische Universität Braunschweig, 38106 Braunschweig, Germany

ARTICLE INFO

Article history:
Received 14 December 2012
Accepted 31 January 2013
Available online 10 February 2013

Keywords:
Continuum mechanics
Inhomogeneous growth
Biology
Finite plasticity theory

ABSTRACT

In general, growth characterises the process by which a material increases in size by the addition of mass. In dependence on the prevailing boundary conditions growth occurs in different, often complex ways. However, in this paper we aim to develop a model for biological systems growing in an inhomogeneous manner thereby generating residual stresses even when growth rates and material properties are homogeneous. Consequently, a descriptive example could be a body featuring homogeneous, isotropic material characteristics that grows against a barrier. At the moment when it contacts the barrier inhomogeneous growth takes place. If thereupon the barrier is removed, some types of bodies keep the new shape mainly fixed. As a key idea of the proposed phenomenological approach, we effort the theory of finite plasticity applied to the isochoric part of the Kirchhoff stress tensor as well as an additional condition allowing for plastic changes in the new grown material, only. This allows us to describe *elastic bodies with a fluid-like growth characteristic*. Prominent examples are tumours where the characteristic macro mechanical growth behaviour can be explained based on cellular arguments. Finally, the proposed framework is embedded into the finite element context which allows us to close this study with representative numerical examples.

1. Introduction

Growth phenomena are defined as material increase in size by the addition of mass and are of sociological interest as they appear in various domains of our daily routine: From cells over tissues to entire organisms. Analyses of such phenomena have entered in many different scientific communities, reaching from classical biology and plant biology over medical sciences to engineering and mathematics. The common aim of all these scientific groups is a detailed understanding of growth behaviour for most diverse processes including e.g. plant growth (Srivastava, 2002; Beck, 2010), wound healing (Martin, 1997; Thackham et al., 2008), bone regeneration (Dimitriou et al., 2011; Tal, 2012), tumour growth (Kim et al., 2011), aneurysms growth (Keen and Dobrin, 2000), and in general growth of tissues such as arteries (Helisch and Schaper, 2003), skeletal muscles (Koopman and van Loon, 2009), or heart (Burggren and Keller, 1997; Tomanek and Runyan, 2001), to list only a few obvious examples. However, growth fulfils a variety of biological functions and takes place in three typical forms, namely tip growth, surface growth, and volume growth (BenAmar and Goriely, 2005). In contrast to tip and surface growth, volumetric growth in the bulk of biological systems has been well-documented as it occurs in most systems such as arteries,

*Corresponding author.
E-mail address: m.boel@tu-bs.de (M. Böl).

1751-6161/$ - see front matter © 2013 Elsevier Ltd. All rights reserved.
http://dx.doi.org/10.1016/j.jmbbm.2013.01.027

skeletal muscles, heart, airways, and solid tumours (Taber, 1995; Ambrosi and Mollica, 2002; Humphrey, 2003; Cowin, 2004; Moulton and Goriely, 2011; Dervaux and Ben Amar, 2011).

After the perception that soft tissues are highly complex materials, featuring non-linear, anisotropic, and inhomogeneous characteristics, significant endeavours have been directed toward the development of theoretical models for volumetric growth, mostly for soft tissues such as cardiac tissue (Kroon et al., 2009; Göktepe et al., 2010b), tendons (Garikipati et al., 2004), skeletal muscles (Zöllner et al., 2012), tumours (Ambrosi and Mollica, 2002), and vascular tissues (Taber and Humphrey, 2001; Alastrué et al., 2008). However, all these models follow the general statement of growth (Rodriguez et al., 1994) in terms of the multiplicative decomposition of the geometrical deformation gradient as known from elasto-plasticity (Kröner, 1959; Lee, 1969). Basic idea of Rodriguez et al. (1994) is that the deformation gradient is split into a growth part describing the local exchange of mass and a so-called elastic one to ensure compatibility and integrity due to growth. As the deformation gradient is a geometric tensor, the modelling of growth using the multiplicative decomposition is of geometric nature, too. This fact initiated a discussion about the suitability of this approach, see Humphrey and Rajagopal (2002) and Ambrosi et al. (2011). Following Humphrey and Rajagopal (2002), a possible remedy could be the modelling of growth within the mixture theory. Growth could be then described by the evolution of various natural configurations. However, the majority of contributions use the classic multiplicative decomposition of the deformation gradient.

An intensive discussed phenomenon in terms of volumetric growth is the generation of residual stresses inside biological systems (Hoger, 1986; Skalak et al., 1996). Basically, when growth takes place locally, e.g. due to local nutrient supply (Ambrosi and Preziosi, 2012), parts of the body become stretched/compressed to ensure compatibility. These strains are associated with stresses referred to as residual stresses which have been shown to play an important role in the function of soft tissues. The maybe most prominent example in this respect are residual stresses in arteries regulating the stress distribution inside the arterial wall (Rachev and Greenwald, 2003).

In this paper, we aim to study biological systems that grow in an inhomogeneous manner thereby generating residual stresses even when material characteristics are homogeneous. Such growth scenarios are known e.g. from cells (Ateshian and Humphrey, 2012) or tumours (Ambrosi and Preziosi, 2012). However, in order to become more familiar with inhomogeneous growth driven by external constraints, the basic idea is demonstrated on an apple, see Fig. 1. Hereby, a cable tie was attached to the apple during the growth process, see Fig. 1(a). After a growth period of two months the apple was picked and a photo was made directly from this situation, see (b). Alter slicing the cable tie it springs open and by merging both ends a distance ΔL, cf. (c), could be detected. In (d) the bisected apple is illustrated. Two effects can be observed: first, due to the restriction imposed by the cable tie, the apple is prevented to grow homogeneously although its flesh can be characterised to be isotropic and homogeneous (apart from the apple core). This behaviour leads to rank growth especially in the region around the cable tie, cf. (b) and (d). The second effect can be visualised when focusing on the distance ΔL. The burst of the cable tie when cut points out that there are some residual stresses inside the apple. As the mechanical behaviours of the apple and the cable tie are

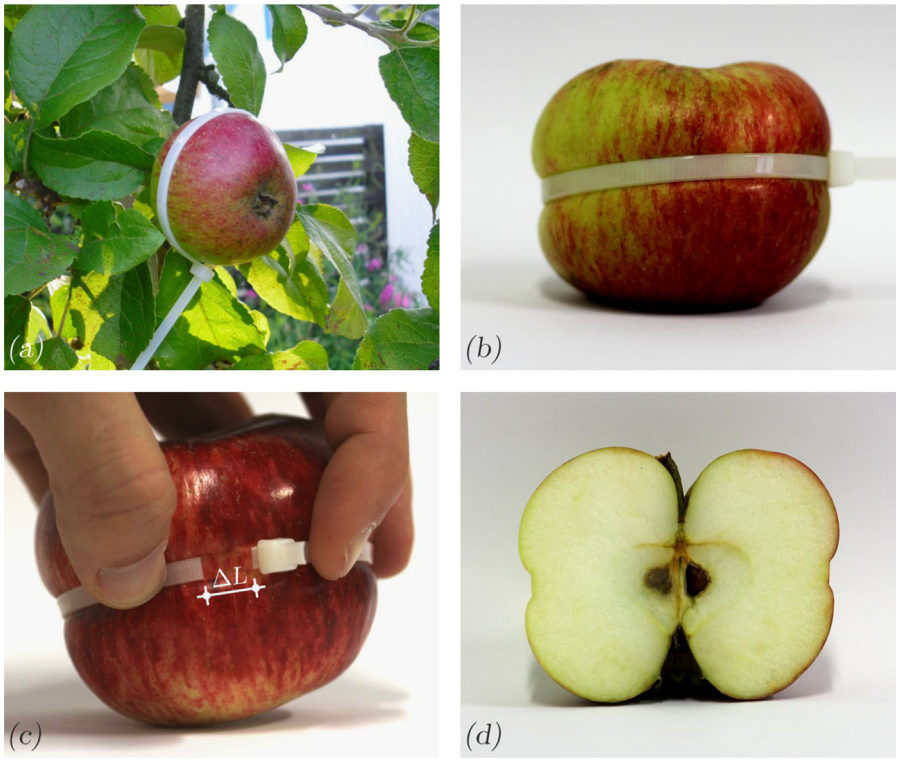

Fig. 1 – Inhomogeneous, locally restricted growth of an apple. (a) Situation on the tree, a cable tie has been loosely attached around an apple. (b) Apple after two months of growth, (c) cut cable tie, and (d) same apple bisected.

unknown we cannot make a point about the quantity of the residual stresses. However, as the shape change of the apple between the situation with (b) and without (c) cable tie is marginal, we suggest that the residual stresses are small, too.

Such behaviour poses, similar to tumours Ambrosi and Preziosi (2012), the question: *How do such materials grow?* From the macro mechanical point of view it seems clear that these materials behave like a solid towards external loads. On the other hand, when a solid with a fixed growth direction grows against an external constraint, residual stresses are generated. The solid would adapt the multiple of its reference geometry when removing the constraint. However, in case of the apple example a different type of growth appears as the apple does not return to an isotropically grown reference geometry when cut the cable tie, see Fig. 1(d). That leads to the idea that such biological systems grow with fluid-like characteristics although they exhibit the material behaviour of a solid. Consequently, stress relaxation occurs and therefore residual stresses decrease. Thereby the amount of stresses can vary depending on the biological systems' material characteristics. In case of tumours, the aforementioned characteristic behaviour observed at macro scale can be explained rooted on cellular argument. Following Ambrosi and Preziosi (2009), during growth new cell aggregates develop and lead to cell reorganisation and thus to stress relaxation at macro level. In other words when a certain yield value is reached the cells reorganise and thus the solid grows inhomogeneously in a relaxed manner similar to the apple example. However, at macro level such behaviour can be described in terms of finite plasticity theory, see also Bolea Albero et al. (2012).

2. Continuum modelling of inhomogeneous growth

In this section, we illustrate the governing equations for inhomogeneous growth of solid bodies. In what follows, the kinematic equations rooted on the multiplicative decomposition of the deformation gradient tensor are outlined, see Section 2.1. Before in Section 2.3 the constitutive equations as well as the specific stress measures are presented, the balance equations of open systems are stated in Section 2.2. Finally, Section 2.4 is devoted to the numerical determination of the modified growth deformation tensor responsible for inhomogeneous growth.

2.1. Kinematics for finite growth

To characterise finite growth, we introduce the incompatible growth configuration $\hat{\mathcal{B}}$ and apply the multiplicative decomposition of the deformation gradient $\boldsymbol{F}$ into an elastic $\boldsymbol{F}_e$ and a growth part $\boldsymbol{F}_g$ (Rodriguez et al., 1994)

$$\boldsymbol{F} = \boldsymbol{F}_e \boldsymbol{F}_g \quad \text{with } \boldsymbol{F} = \nabla_X \boldsymbol{\varphi}(\boldsymbol{X}, t), \tag{1}$$

a concept first proposed in the context of finite elastoplasticity (Kröner, 1959; Lee, 1969). Herein, the spatial gradient with respect to the undeformed coordinates $\boldsymbol{X}$ is characterised by ∇_X. Based on the concept of classical continuum mechanics, $\boldsymbol{\varphi}$ is the deformation map, mapping at any time t the material placement $\boldsymbol{X}$ of a material particle in the reference configuration $\mathcal{B}_0$ to its spatial placement $\boldsymbol{x}$ in the current configuration $\mathcal{B}$. Accordingly, the total Jacobian

$$J = \det \boldsymbol{F} = J_e J_g \tag{2}$$

responds a similar multiplicative split into an elastic $J_e = \det \boldsymbol{F}_e$ and a growth part $J_g = \det \boldsymbol{F}_g$. Motivated by biological/physiological observations during growth (cf. Section 1), we aim to define a numerical scheme to evaluate $\boldsymbol{F}_g$, see Section 2.4. Consequently, a few mathematical relations have to be defined before. In doing so, we introduce the left Cauchy Green strain tensor $\boldsymbol{b}$ and its elastic counterpart $\boldsymbol{b}_e$ as

$$\boldsymbol{b} = \boldsymbol{F}\boldsymbol{F}^T \quad \text{and} \quad \boldsymbol{b}_e = \boldsymbol{F}_e \boldsymbol{F}_e^T, \tag{3}$$

to be the characteristic deformation measures. Finally, the mass elements

$$dM = \rho_0 \, dV \quad \text{and} \quad dm = \rho \, dv = \rho_e \, d\hat{V} = \rho_g \, dV, \tag{4}$$

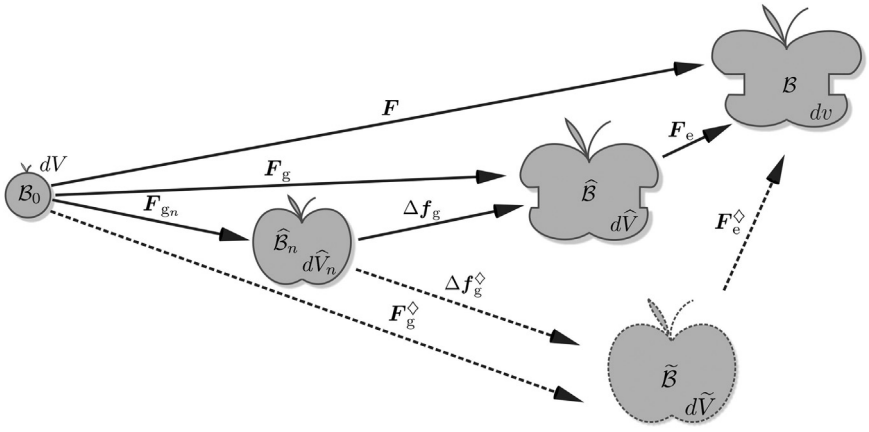

Fig. 2 – Multiplicative decomposition of the deformation gradient F. The reference and current configurations are characterised by $\mathcal{B}_0$ and $\mathcal{B}$. Further, there exist two intermediate configurations, one $\hat{\mathcal{B}}$ at the current time t and another one $\hat{\mathcal{B}}_n$ at the end of the previous time step t_n. Finally, the last configuration $\tilde{\mathcal{B}}$ can be called 'test' configuration as is represents the isotropic expansion of the intermediate configuration $\hat{\mathcal{B}}_n$ due to the growth deformation update $\Delta f_g^\diamond$, see Eq. (18). Accordingly, the volume elements dV, dv, $d\hat{V}$ (and $d\hat{V}_n$), and $d\tilde{V}$ are defined in the reference, current, intermediate, and 'test' configuration, respectively.

in the reference and the current configuration depend on the volume elements dV, $d\hat{V}$ and dv as well as on the densities ρ_0, ρ_e and ρ in the reference, intermediate, and current configuration, respectively, see also Fig. 2. From Eq. (4) it follows that the relation between the mass element in the current and the volume element in the reference configuration is referred to as the grown density $\rho_g = dm/dV$.

2.2. Balance equation of open systems

Using the framework of open system thermodynamics in which the grown density ρ_g is allowed to change (Kuhl and Steinmann, 2003) the balance of mass

$$\dot{\rho}_g = \mathrm{Div}\,\mathbf{R} + \mathcal{R}_0, \tag{5}$$

balances its rate of change $\dot{\rho}_g$ with a possible in- or outflux of mass $\mathbf{R}$ and a mass term $\mathcal{R}_0$. The operator Div(•) denotes the divergence with respect to the coordinates $\mathbf{X}$ in the reference configuration. Assuming that the mass changes due to diffusion are significantly smaller than local changes in mass we suppose $\mathbf{R} = \mathbf{0}$ and thus Eq. (5) simplifies as

$$\dot{\rho}_g = \mathcal{R}_0. \tag{6}$$

Further, we define the specific growth rate

$$\Gamma = \frac{\dot{dm}}{dm} = \frac{\dot{\rho}_g}{\rho_g} = \text{const.}, \tag{7}$$

to be either the ratio between $\dot{dm}$ and dm or alternatively, using the time derivative of Eq. $(4)_2$, to be the ratio between $\dot{\rho}_g$ and ρ_g. Finally, inserting Eq. (7) into (5) we conclude with

$$\dot{\rho}_g = \Gamma \rho_g, \tag{8}$$

to be the specific balance of mass used in the present contribution. Note, that ρ_g depends on time, thus depicts a non-constant quantity.

Similarly, in absence of transient terms and external forces, the balance of linear momentum can be expressed as

$$\mathrm{div}(J^{-1}\boldsymbol{\tau}) = \mathbf{0}, \tag{9}$$

where $\boldsymbol{\tau}$ is the Kirchhoff stress and the operator div(•) denotes the spatial divergence with respect to the spatial position $\boldsymbol{\varphi}$.

2.3. Constitutive equations

Due to the high amount of water in living tissues it is justified to assume incompressible material behaviour. In computational mechanics it is often convenient to allow for slight volumetric changes and accordingly, to consider near-incompressible material. The basic step for this procedure is a multiplicative split of the total elastic deformation into volumetric and isochoric parts as Flory (1961)

$$\mathbf{F}_e = (J_e^{1/3})\overline{\mathbf{F}}_e, \tag{10}$$

where $\overline{\mathbf{F}}_e$ is the isochoric portion. As a consequence, the elastic volume-preserving part $\overline{\boldsymbol{b}}_e = (J_e^{-2/3})\boldsymbol{b}_e$ of the elastic left Cauchy Green tensor follows from Eq. $(3)_2$. Accordingly, we use the additive decomposition of the Helmholtz free energy

$$\psi = \psi_{\mathrm{iso}}(\overline{\boldsymbol{b}}_e) + \psi_{\mathrm{vol}}(J_e), \tag{11}$$

into a volume-preserving contribution $\psi_{\mathrm{iso}}(\overline{\boldsymbol{b}}_e)$ and the volumetric portion $\psi_{\mathrm{vol}}(J_e)$. Finally, the Kirchhoff stress

$$\boldsymbol{\tau} = \boldsymbol{\tau}_{\mathrm{iso}} + \boldsymbol{\tau}_{\mathrm{vol}} = 2\rho_g\,\mathrm{dev}\left(\overline{\boldsymbol{b}}_e \frac{\partial \psi_{\mathrm{iso}}(\overline{\boldsymbol{b}}_e)}{\partial \overline{\boldsymbol{b}}_e}\right) + \rho_g J_e \frac{\partial \psi_{\mathrm{vol}}(J_e)}{\partial J_e}\mathbf{I}, \tag{12}$$

to be the thermodynamically conjugate quantity to the elastic left Cauchy Green tensor $\overline{\boldsymbol{b}}_e$ can be likewise expressed in the decoupled form, whereby $\boldsymbol{I}$ is the second order identity tensor and the expression $\mathrm{dev}(\bullet) = (\bullet) - 1/3\,\mathrm{tr}(\bullet)\boldsymbol{I}$ denotes the deviatoric operator.

2.4. Numerical determination of $\mathbf{F}_g$ for fluid-like growth characteristics

In contrast to several growth models where the growth deformation tensor $\mathbf{F}_g$ is predefined, e.g. using a scalar-valued growth multiplier (Ambrosi and Preziosi, 2012), the aim of the present section is a numerical determination of the growth deformation tensor for fluid-like materials as well as elastic materials that feature fluid-like growth characteristics.

Before presenting the approach in detail, some general definitions must be indicated. Consequently, quantities for a given deformation state at the current time t and those at the end of the previous time step t_n need to be determined. In what follows, we insert the time derivative of Eq. $(4)_2$ in (8) which leads under assumption of constant density during growth, e.g. $\rho_e = \rho_0 = \text{const.}$, to

$$\dot{d\hat{V}} = \Gamma\, d\hat{V}, \tag{13}$$

presenting the specific growth rate in dependence on the current volume element $d\hat{V}$ and the previous one $d\hat{V}_n$ in the intermediate configurations $\hat{\mathcal{B}}$ and $\hat{\mathcal{B}}_n$, respectively. Its solution

$$d\hat{V} = d\hat{V}_n \exp(\Gamma\,\Delta t), \tag{14}$$

is presented in a finite difference scheme, where $\Delta t := t - t_n > 0$. For further use we define

$$j_g = \frac{d\hat{V}}{d\hat{V}_n}, \tag{15}$$

being the ratio between the current and the previous volume elements in the respective intermediate configurations.

2.4.1. Fluid-like growing materials

The evolution of the growth deformations is defined by means of a multiplicative split of the growth deformation gradient

$$\mathbf{F}_g = \Delta\boldsymbol{f}_g \mathbf{F}_{g_n}, \tag{16}$$

into the previous growth deformation gradient $\mathbf{F}_{g_n}$ and its update $\Delta\boldsymbol{f}_g$, see also Fig. 2.

With the update of the growth deformation gradient at hand, the volume change is expressed via the growth Jacobian

$$J_g = \det(\mathbf{F}_g) = j_g J_{g_n} \quad \text{with } J_{g_n} = \det(\mathbf{F}_{g_n}) = \frac{d\hat{V}_n}{dV}. \tag{17}$$

As the determination of the growth deformation gradient requires a numerical iteration scheme, we define all non-converged quantities with a diamond, i.e. $(\bullet)^{\diamond}$, and specify an isotropic increment for the growth deformation update

$$\Delta\boldsymbol{f}_g^{\diamond} = j_g^{1/3}\boldsymbol{I}. \tag{18}$$

Inserting Eq. (18) in the non-converged expressions of the deformation gradient $(1)_1$ and its growth part (16), i.e. $\boldsymbol{F}=\boldsymbol{F}_{\mathrm{e}}^{\diamond}\boldsymbol{F}_{\mathrm{g}}^{\diamond}$ and $\boldsymbol{F}_{\mathrm{g}}^{\diamond}=\Delta\boldsymbol{f}_{\mathrm{g}}^{\diamond}\boldsymbol{F}_{\mathrm{g}_n}$, the non-converged elastic deformation gradient reads

$$\boldsymbol{F}_{\mathrm{e}}^{\diamond}=\boldsymbol{F}(\boldsymbol{F}_{\mathrm{g}}^{\diamond})^{-1}=\boldsymbol{F}\boldsymbol{F}_{\mathrm{g}_n}^{-1}j_{\mathrm{g}}^{-1/3}=\boldsymbol{F}\boldsymbol{F}_{\mathrm{g}_n}^{-1}[\exp(\Gamma\,\Delta t)]^{-1/3}. \tag{19}$$

With the elastic deformation gradient at hand, the Kirchhoff stress tensor

$$\boldsymbol{\tau}^{\diamond}=\boldsymbol{\tau}_{\mathrm{iso}}^{\diamond}+\boldsymbol{\tau}_{\mathrm{vol}}^{\diamond}=2\rho_{\mathrm{g}}\,\mathrm{dev}\left(\overline{\boldsymbol{b}}_{\mathrm{e}}^{\diamond}\frac{\partial\psi_{\mathrm{iso}}(\overline{\boldsymbol{b}}_{\mathrm{e}}^{\diamond})}{\partial\overline{\boldsymbol{b}}_{\mathrm{e}}^{\diamond}}\right)+\rho_{\mathrm{g}}J_{\mathrm{e}}^{\diamond}\frac{\partial\psi_{\mathrm{vol}}(J_{\mathrm{e}}^{\diamond})}{\partial J_{\mathrm{e}}^{\diamond}}\boldsymbol{I}, \tag{20}$$

straightforwardly results in its non-converged format using the modification of the left Cauchy Green tensor $(3)_2$, i.e. $\boldsymbol{b}_{\mathrm{e}}^{\diamond}=\boldsymbol{F}_{\mathrm{e}}^{\diamond}(\boldsymbol{F}_{\mathrm{e}}^{\diamond})^{T}$, and the elastic non-converged Jacobian which is, due to preserving volume flow of the body, identical to the converged one, i.e. $J_{\mathrm{e}}^{\diamond}=J_{\mathrm{e}}$, $\det(\Delta\boldsymbol{f}_{\mathrm{g}}^{\diamond})=\det(\Delta\boldsymbol{f}_{\mathrm{g}})$, and $d\tilde{V}=d\hat{V}$. Further, we define

$$\dot{\boldsymbol{\tau}}_{\mathrm{e,iso}}=-K\boldsymbol{\tau}_{\mathrm{e,iso}}\quad\text{with }\boldsymbol{\tau}_{\mathrm{e,iso}}=2\,\mathrm{dev}\left(\overline{\boldsymbol{b}}_{\mathrm{e}}\frac{\partial\psi_{\mathrm{iso}}(\overline{\boldsymbol{b}}_{\mathrm{e}})}{\partial\overline{\boldsymbol{b}}_{\mathrm{e}}}\right), \tag{21}$$

where K is the characteristic relaxations rate and $\dot{\boldsymbol{\tau}}_{\mathrm{e,iso}}$ presents the time derivative of the density-independent isochoric part of the Kirchhoff stress tensor $\boldsymbol{\tau}_{\mathrm{e,iso}}$. We finalise with a representation for the isochoric and volumetric part of the Kirchhoff stress tensor

$$\boldsymbol{\tau}_{\mathrm{iso}}=\boldsymbol{\tau}_{\mathrm{iso}}^{\diamond}\exp(-K\,\Delta t)\quad\text{and}\quad\boldsymbol{\tau}_{\mathrm{vol}}=\boldsymbol{\tau}_{\mathrm{vol}}^{\diamond}, \tag{22}$$

by applying the relationships between the density-independent and density-dependent quantities in the converged $\boldsymbol{\tau}_{\mathrm{e,iso/vol}}=1/\rho_{\mathrm{g}}\boldsymbol{\tau}_{\mathrm{iso/vol}}$ as well as in the non-converged $\boldsymbol{\tau}_{\mathrm{e,iso/vol}}^{\diamond}=1/\rho_{\mathrm{g}}\boldsymbol{\tau}_{\mathrm{iso/vol}}^{\diamond}$ format.

Following Simo and Ortiz (1985), $\overline{\boldsymbol{F}}_{\mathrm{e}}$ can be computed numerically from $\boldsymbol{\tau}_{\mathrm{iso}}$ under the assumption of an isotropic elastic behaviour, as the deformation gradient is defined by its stretch, thus $\overline{\boldsymbol{F}}_{\mathrm{e}}=\overline{\boldsymbol{V}}_{\mathrm{e}}=\overline{\boldsymbol{b}}_{\mathrm{e}}^{1/2}$. Eventually, using Eqs. $(1)_1$ and (10) we end up with the target value $\boldsymbol{F}_{\mathrm{g}}$.

2.4.2. *Inhomogeneous growth of elastic materials*

The application of a flow rule, as introduced in Eq. $(21)_1$, implies an uncontrolled flow of the material during loading. Such behaviour is known related to biofilms (e.g. Böl et al., in press). However, in order to ensure only a flow of the new grown material contribution at the current time increment, the principal values $\lambda_{\Delta\mathrm{g,i}}$ in the corresponding directions $\hat{\boldsymbol{n}}_{\mathrm{i}}$ and $\hat{\boldsymbol{n}}_{\mathrm{i}_n}$ of the spectrally decomposed growth update tensor

$$\Delta\boldsymbol{f}_{\mathrm{g}}=\sum_{\mathrm{i}=1}^{3}\lambda_{\Delta\mathrm{g,i}}\hat{\boldsymbol{n}}_{\mathrm{i}}\otimes\hat{\boldsymbol{n}}_{\mathrm{i}_n}, \tag{23}$$

need to fulfil the condition

$$1\leq\lambda_{\Delta\mathrm{g,i}}. \tag{24}$$

In case this condition is not satisfied, the relaxation rate

$$K=K^{m}+\Delta K, \tag{25}$$

has to be updated within the Newton–Raphson's method, using the initial value K^0. Note, due to clarity reasons, quantities of the previous iteration have been indexed by m whereas for current values we omit the index instead of using $m+1$. In what follows, the discrete residual equation

$$r=\lambda_{\min}-1. \tag{26}$$

has been established. Herein, $\lambda_{\min}=\min(\lambda_{\Delta\mathrm{g,i}})$ is the minimum principal value. The update of the characteristic relaxation rate

$$\Delta K=-r\left[\frac{\partial K}{\partial r}\right]_{K}=-r\left[\frac{\partial K}{\partial\boldsymbol{b}_{\mathrm{e}}}:\frac{\partial\boldsymbol{b}_{\mathrm{e}}}{\partial\boldsymbol{C}_{\mathit{\Delta}}}:\frac{\partial\boldsymbol{C}_{\mathit{\Delta}}}{\partial r}\right]_{K}, \tag{27}$$

can be determined via chain rule, whereby $\boldsymbol{C}_{\mathit{\Delta}}=\Delta\boldsymbol{f}_{\mathrm{g}}^{T}\Delta\boldsymbol{f}_{\mathrm{g}}$ denotes an isotropic update strain tensor featuring quadratic eigenvalues of $\Delta\boldsymbol{f}_{\mathrm{g}}$. Consequently, the first term

$$\frac{\partial K}{\partial\boldsymbol{b}_{\mathrm{e}}}=\frac{\partial K}{\partial\boldsymbol{\tau}_{\mathrm{e,iso}}}:\frac{\partial\boldsymbol{\tau}_{\mathrm{e,iso}}}{\partial\overline{\boldsymbol{b}}_{\mathrm{e}}}:\frac{\partial\overline{\boldsymbol{b}}_{\mathrm{e}}}{\partial\boldsymbol{b}_{\mathrm{e}}}\quad\text{with }\frac{\partial K}{\partial\boldsymbol{\tau}_{\mathrm{e,iso}}}=-\frac{1}{\Delta t}\frac{1}{\tau_{\mathrm{e,iso}}}, \tag{28}$$

on the right-hand side of Eq. (27) is known once the material characteristics (11) are defined. Further, the derivative of the elastic left Cauchy Green strain tensor with respect to the isotropic update strain tensor

$$\frac{\partial\boldsymbol{b}_{\mathrm{e}}}{\partial\boldsymbol{C}_{\mathit{\Delta}}}=-[\boldsymbol{F}\boldsymbol{F}_{\mathrm{g}_n}^{-1}]\cdot\frac{1}{2}[\boldsymbol{C}_{\mathit{\Delta}}^{-1}\overline{\otimes}\boldsymbol{C}_{\mathit{\Delta}}^{-1}+\boldsymbol{C}_{\mathit{\Delta}}^{-1}\underline{\otimes}\boldsymbol{C}_{\mathit{\Delta}}^{-1}]\bigcirc[\boldsymbol{F}_{\mathrm{g}_n}^{-T}\boldsymbol{F}^{T}], \tag{29}$$

can be straightforwardly determined using standard arguments of continuum mechanics. Herein, the tensor products are defined as $\mathbb{A}=\boldsymbol{D}\overline{\otimes}\boldsymbol{E}$, $\mathbb{A}=\boldsymbol{D}\underline{\otimes}\boldsymbol{E}$, and $\mathbb{A}=\mathbb{B}\bigcirc\boldsymbol{D}$ with the indices $A_{ijkl}=D_{ik}E_{jl}$, $A_{ijkl}=D_{il}E_{jk}$, and $A_{ijkl}=B_{imkl}D_{mj}$, respectively. Finally, following Mosler and Meschke (2003) the derivation of the deformation gradient update with respect to the residuum simplifies to

$$\frac{\partial\boldsymbol{C}_{\mathit{\Delta}}}{\partial r}=\frac{\partial\boldsymbol{C}_{\mathit{\Delta}}}{\partial(\lambda_{\min}^{2})}2\lambda_{\min}. \tag{30}$$

Summarising, this set of equations allows the determination of $\Delta\boldsymbol{f}_{\mathrm{g}}$, see local Newton update in Table 1, and finally in consideration of Eq. (16), the determination of the growth deformation gradient.

Table 1 – Local Newton update of the internal variable $\Delta\boldsymbol{f}_{\mathrm{g}}$.

Given are $\boldsymbol{\tau}_{\mathrm{iso}}^{\diamond}$,$\boldsymbol{F}$,$\boldsymbol{F}_{\mathrm{g}_n}$, and K^0

Computation of:	
(1)	isochoric part of the Kirchhoff stress tensor $\boldsymbol{\tau}_{\mathrm{iso}}$
(2)	elastic, left Cauchy Green tensor $\overline{\boldsymbol{b}}_{\mathrm{e}}$ from $\boldsymbol{\tau}_{\mathrm{iso}}$
(3)	growth deformation gradient update $\Delta\boldsymbol{f}_{\mathrm{g}}$
(4)	principal values $\lambda_{\Delta\mathrm{g,i}}$ of $\Delta\boldsymbol{f}_{\mathrm{g}}$ and their minimum $\lambda_{\min}$
(5)	check if $\lambda_{\min}\geq 1$
(6)	yes → goto end
(7)	no → continue with algorithm
(8)	while $\lvert r\rvert\geq\mathrm{tol}$ do
(9)	determine the update ΔK and the relaxation rate K
(10)	isochoric part of the Kirchhoff stress tensor $\boldsymbol{\tau}_{\mathrm{iso}}$
(11)	elastic, left Cauchy Green tensor $\overline{\boldsymbol{b}}_{\mathrm{e}}$ from $\boldsymbol{\tau}_{\mathrm{iso}}$
(12)	principal values $\lambda_{\Delta\mathrm{g,i}}$ of $\Delta\boldsymbol{f}_{\mathrm{g}}$ and their minimum $\lambda_{\min}$
(13)	go to (8)
(14)	end while

3. Numerical examples

This section is devoted to illustrative examples in order to demonstrate the key features of the proposed modelling approach. To this end, three boundary problems have been considered. First, in order to make the capability of the modelling concept obvious, we apply uniaxial simulations. Hereby, characteristics have been considered reaching from elastic materials growing in an unvarying, default direction to more advanced materials such as fluids, featuring fluid-like growth behaviour, too. The second example is closely related to the illustration of inhomogeneous cell growth driven by external constraints as discussed in Ateshian et al. (2012). In order to study two issues, namely the influence of elastic constraints on inhomogeneous growth as well as the stable and robust implementation of the growth algorithm within the finite element method, we finally present the example of a solid cylinder growing against a bordering cable tie.

However, as the modelling concept (Section 2) is presented in a more general framework, we initially present the specific forms of the constitutive equations that are utilised in the numerical examples. In doing so, we use the elementary isotropic Neo-Hookean material for the purely mechanical characteristics. Thus, in respect of Eq. (11) we define the isochoric and volumetric part of the Helmholtz free energy as

$$\psi_{\mathrm{iso}}(\bar{\boldsymbol{b}}_{\mathrm{e}}) = \frac{1}{\rho_0}\frac{\mu}{2}(\bar{I}_1 - 3) \quad \text{and} \quad \psi_{\mathrm{vol}}(J_{\mathrm{e}}) = \frac{1}{\rho_0}\frac{B}{2}(J_{\mathrm{e}} - 1)^2, \tag{31}$$

where μ is the shear modulus, B denotes the bulk modulus, and the first invariant arises from $\bar{I}_1 = \mathrm{tr}\,\bar{\boldsymbol{b}}_{\mathrm{e}}$. Once the free energy is specified, the isochoric and volumetric stresses

$$\boldsymbol{\tau}_{\mathrm{iso}} = J_{\mathrm{g}}\mu\,\mathrm{dev}(\bar{\boldsymbol{b}}_{\mathrm{e}}) \quad \text{and} \quad \boldsymbol{\tau}_{\mathrm{vol}} = J_{\mathrm{g}}B(J_{\mathrm{e}}^2 - J_{\mathrm{e}})\boldsymbol{I}, \tag{32}$$

result from Eq. (12) and the isochoric elastic stress as well as its purely isochoric part in the non-converged set-up

$$\boldsymbol{\tau}_{\mathrm{e,iso}} = \frac{1}{\rho_0}\mu\,\mathrm{dev}(\bar{\boldsymbol{b}}_{\mathrm{e}}) \quad \text{and} \quad \boldsymbol{\tau}_{\mathrm{iso}}^{\diamond} = J_{\mathrm{g}}\mu\,\mathrm{dev}(\bar{\boldsymbol{b}}_{\mathrm{e}}^{\diamond}), \tag{33}$$

are determined from Eqs. $(21)_2$ and (22). Finally, with the knowledge of the specified free energy (31) at hand we are able to indicate the second and third term of Eq. $(28)_1$ to be

$$\frac{\partial \boldsymbol{\tau}_{\mathrm{e,iso}}}{\partial \bar{\boldsymbol{b}}_{\mathrm{e}}} = \frac{1}{\rho_0}\mu\left(\mathbb{I} - \frac{1}{3}\boldsymbol{I}\otimes\boldsymbol{I}\right) \quad \text{and} \quad \frac{\partial \bar{\boldsymbol{b}}_{\mathrm{e}}}{\partial \boldsymbol{b}_{\mathrm{e}}} = J_{\mathrm{e}}^{-2/3}\left(\mathbb{I} - \frac{1}{3}\boldsymbol{b}_{\mathrm{e}}\otimes\boldsymbol{b}_{\mathrm{e}}^{-1}\right), \tag{34}$$

whereby $\mathbb{I}$ denotes the fourth-order identity tensor.

Unless stated otherwise, for the following numerical examples the parameters as given in Table 2 are specified.

Table 2 – Material parameters for the numerical examples. Note, upper index (i)/(ii)/(iii) of μ, defining the shear modulus of the cable ties, correlates with the results in Fig. 8.

Parameter	Value	Unit
General analyses (Section 3.1)		
μ	100	Pa
B	1×10^6	Pa
K	0/0.005/0.05	s^{-1}
Γ	0.005	s^{-1}
Inhomogeneous growth: rigid constraints (Section 3.2)		
μ	100	Pa
B	1×10^6	Pa
K	0.05	s^{-1}
Γ	0.005	s^{-1}
Inhomogeneous growth: elastic constraints (Section 3.3)		
Growing cylinder:		
μ	100	Pa
B	1×10^6	Pa
K	0/0.005/0.05	s^{-1}
Γ	0.005	s^{-1}
Cable ties:		
$\mu^{(\mathrm{i})/(\mathrm{ii})/(\mathrm{iii})}$	$3.3 \times 10^2/3.3 \times 10^3/3.3 \times 10^4$	Pa
B	1.7×10^6	Pa

3.1. General performance of the growth approach

In order to reveal the basic characteristics of the presented growth model in this section, we consider a three-dimensional cubic solid discretised with 27 hybrid linear hexahedra elements. The solid is mounted in a uniaxial way whereby the pressure load $p(t)$ is applied in 3-direction. The temporal sequence of $p(t)$ and the growth activation are characterised by two graphs, see Fig. 3.

The results are illustrated in Fig. 4. Herein, four scenarios have been studied, while keeping the specific growth rate Γ constant (leading to a 2.7-fold volume growth) the relaxation rate K has been varied between 0 and 0.05 s^{-1}, see caption Fig. 4.

For the first case (a) the omission of the relaxation rate leads to classical isotropic growth characterised by the fact that all three principal values $\lambda_{\mathrm{g,i}}$ of the growth deformation gradient $\boldsymbol{F}_{\mathrm{g}}$ are identical. Thus, the body behaves like an elastic solid that grows isotropically, i.e. after unloading the body deforms back to a cube with a 2.7-fold initial volume.

Alternatively, to reach the other end of the scale, i.e. to describe a fluid with fluid-like growth characteristics, we have chosen the relaxation rate to be $K = 0.05\ s^{-1}$ and neglected restriction (24). In that case $\lambda_{\mathrm{g},1/2}$ increase drastically whereas $\lambda_{\mathrm{g},3}$ develops to be smaller than one, see (d). Further, the principal values λ_{i} of the deformation gradient $\boldsymbol{F}$ develop qualitatively similar. There findings suggest that the material flows in the direction with less resistance, i.e. in 1/2-direction. Finally, by removing the pressure load the body deforms back very marginal, only.

These two border cases demonstrate the limits of the present modelling approach. In contrast to the purely isotropic growth case (a), for sample (b) a relaxation rate of $K = 0.005\ s^{-1}$ has been used. The result is a translocation of the growth orientation in 1/2-direction, see Fig. 4(b). In fact the material grows more than it flows (restriction (24) is always satisfied without an update of K) and thus describes the converse behaviour in comparison to case (c) with $K = 0.05\ s^{-1}$, where restriction (24) is fulfilled based on the update of K. However, the material does not grow in 3-direction as it is 'easier' to grow in the other directions. Further, when removing the external load, the body in example (b) removes back as indicated by the progress of λ_3 whereas in (c) no recovery is visible.

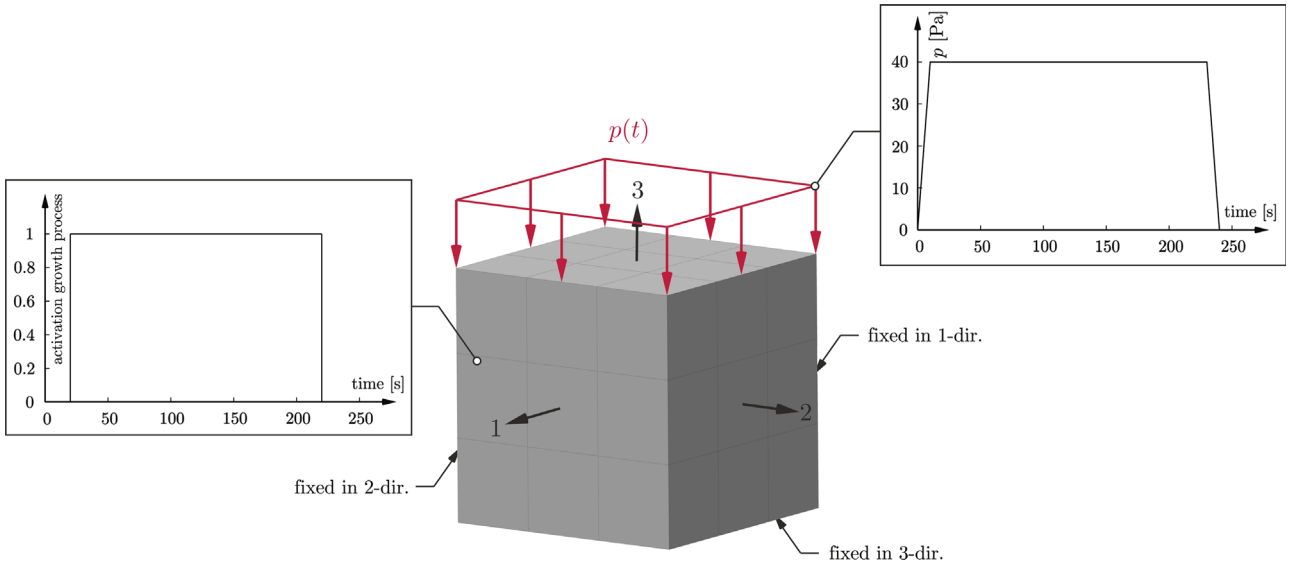

Fig. 3 – System and boundary conditions. The solid is loaded by a maximum pressure load of 40 Pa over a time period of 220 s while growth occurs for a time interval of 200 s, only.

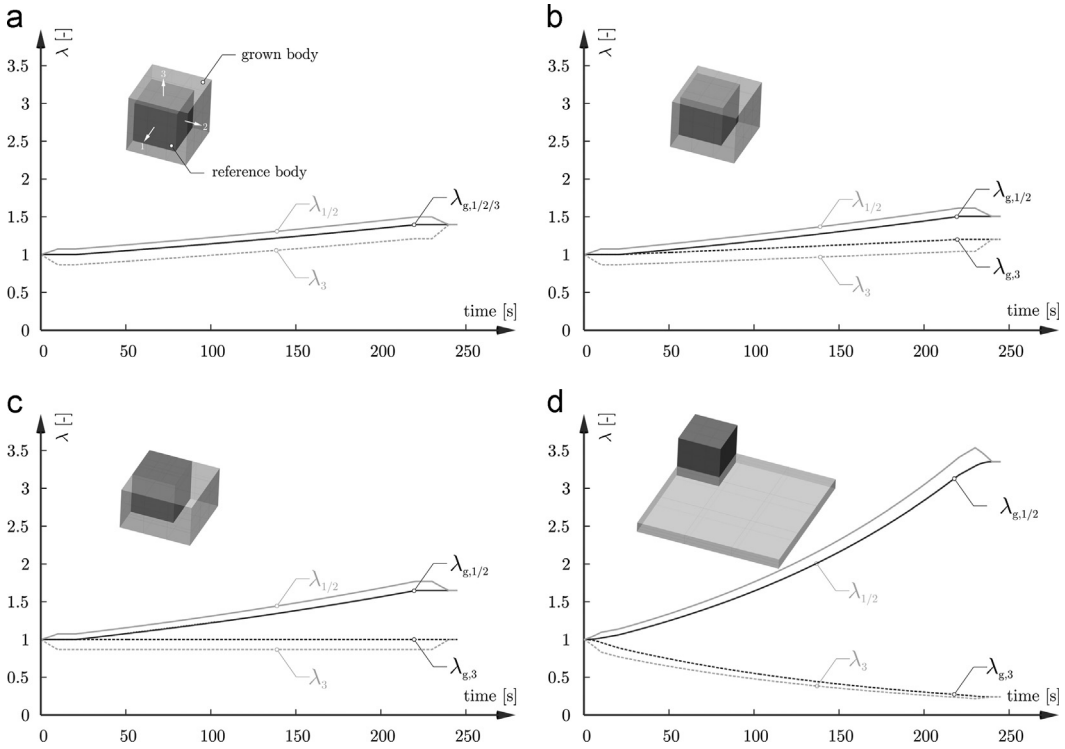

Fig. 4 – Results of the analyses for a constant specific growth rate and a relaxation rate of (a) $K=0\ s^{-1}$, (b) $K=0.005\ s^{-1}$, (c) $K=0.05\ s^{-1}$, and (d) $K=0.05\ s^{-1}$. Note, while for cases (a) and (b) restriction (24) is satisfied automatically, case (c) needs the update of the relaxation rate in order to fulfil this restriction. For case (d), relation (24) is not considered. Illustrated are the principal values λ_i of the deformation gradient F and the ones $\lambda_{g,i}$ of the growth deformation gradient F_g, where $i=1$–3. Further, the sub-figures illustrate the reference (dark grey) and grown bodies (light grey) at time step $t=250$ s.

On the other hand, when using one parameter set, e.g. the one of case (c), it is also possible to enforce a transition of the growth characteristics towards case (b) while increasing the external load $p(t)$. In more detail, for lower loads the body may grow faster than the material can flow, thereby relation (24) is always satisfied. But, a further increase of $p(t)$ leads to a transition to case (b) as the new grown material flows completely in 1/2-direction and thus escapes from the external load. This, on the other hand, requires a numerical determination of the relaxation rate in terms of local Newton iteration scheme as suggested in Table 1.

3.2. *Externally constrained growth*

Although material properties and growth rates of a body are homogeneous, externally constraints can induce inhomogeneous growth. Motivated by the discussion of externally constrained growth of cells (Ateshian and Humphrey, 2012; Ateshian et al., 2012) or tumours (Ambrosi and Mollica, 2002; Ambrosi and Preziosi, 2012) in this section we follow a slightly modification of an example discussed by Ateshian et al. (2012). Herein, a sphere is located between two external constraints, see Fig. 5.

Before the focus is set on the implications of the external constraints on the growth characteristics, some general remarks on the simulation procedure have to be stated. In doing so, the analysis starts with the initial sphere, cf. Fig. 5(a). During a first period the sphere grows isotropically (b) whereby further growth leads to contact of the sphere with the upper constraint inducing inhomogeneous growth, see (c). Finally, the upper constraint will be removed.

The main variables, i.e. the relaxation rate K, the growth principal value ratio Λ_g, and the equivalent von Mises stress σ_{vM} have been tracked during the growth process and their distribution is illustrated for four discrete time steps $t=244/600/900/930$ s. In order to estimate the growth process we introduce the quantity $\Lambda_g=\lambda_{g\,min}/\lambda_{g\,max}$ which is the ratio between minimum and maximum principal values of the growth deformation gradient. This quantity allows to make a statement about the growth characteristics, i.e. if the material grows in a purely isotropic manner ($\Lambda_g=1.0$) or not ($\Lambda_g<1.0$). During a first growth period of 244 s the sphere develops isotropically and consequently increases its volume 3.4-fold, see row 1. At time step $t=245$ s the sphere contacts the upper constraint inducing inhomogeneous growth (rows 2–3), leading to a 90-fold volume increase (row 3). After a total period of 900 s growth was stopped and the upper constraint was removed in space of 30 s (row 4). In dependence on the relaxation rate K the grown sphere deforms back, see differences in the shapes between rows 3 and 4. In the present case (i.e. $K=0.005\ s^{-1}$, cf. Table 2) this leads to an increase of the height of approximately 15% related to the height at time step $t=900$ s.

Focusing first on the time period of isotropic growth (0–244 s) it stands out, that all variables are characterised by constant values being identical at any spatial point, respectively. This type of growth defines the classical behaviour,

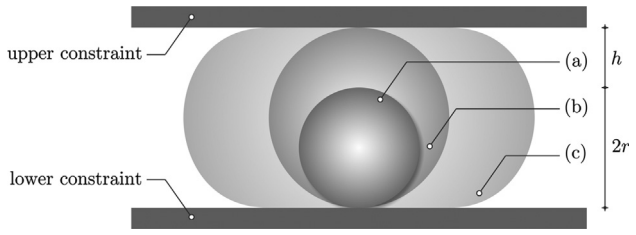

Fig. 5 – Schematic illustration of constrained sphere growth. The sphere with radius $r=0.025$ m is located on the lower constraint. Further, a gap of $h=r$ has been insured between the sphere and the upper constraint. (a) Initial sphere, (b) isotropic grown sphere, and (c) sphere after contacting the upper constraint.

featuring both, homogeneous and isotropic characteristics during growth, see e.g. Ambrosi and Mollica (2002). Based on the contact between sphere and the upper constraint inhomogeneous growth is induced which is reflected by an inhomogeneous distribution of the main variable, see rows 2–3. Starting with the development of the relaxation rate K, pointing to the degree how strong a material flows, it is obvious that the material located at the outer region of the sphere shows less flow characteristics as in the core, see Fig. $6_{A2–A3}$. Especially in the regions without any constraint the maximum value of K is reached. Note, after removing the upper constraint (A4) no distribution of K is available as the growth process has been stopped.

During the first growth period (B1) the growth principal value ratio Λ_g is constant featuring at every spatial point a value of 1.0, and thus approves isotropic growth characteristics. During the second growth period (B2–B3) the sphere shows at the outer region more isotropic growth characteristics than in the core, where a minimum value of $\Lambda_g=0.2$ is reached (B3). While in the first period of inhomogeneous growth (B2) the amount of isotropic growing material, especially on the non-constrained area, is higher, at the end of the growth period (B3) the amount of non-isotropically grown material prevails.

Finally, the equivalent von Mises stress is qualitatively similar distributed as the relaxation rate. The maximum values appear in the core of the sphere (C2–C3) and reach values approximately of 18 Pa. After removing the upper constraint (C4) small residual stresses are visible, only.

3.3. *Inhomogeneous growth due to elastic constraints*

While the latter example focuses on the influence of rigid constraints on the growth behaviour, in this example the influence of elastic boundary conditions on growth is studied. To this end, we follow a slightly modified version of the apple example in Section 1 and assume a growing cylinder constrained by an elastic cable tie. The main idea is to obtain different growth directions in the same body. The material in the constrained area will change its growth direction while the one in the non-constrained region grows more isotropically. This example is not only an impressive example for inhomogeneous growth but demonstrates the computational robustness of the material model and its implementation within the finite element method.

In Fig. 7 a two-dimensional illustration of the geometry as well as the finite element discretisation of an eighth is illustrated. The cylinder grows over 300 s, thereby increasing its volume 4.5-fold. Three types of cable ties, differ from each other by their rigidities, have been considered using the Neo-Hookean material law. The used parameters are summarised in Table 2.

In Fig. 8(a) the development of the radius r, cf. also subfigure (i), in dependence on the time is illustrated for all three parameter sets (i), (ii), and (iii), see Table 2.

Further, for every parameter set the maximum grown geometry is illustrated in combination with the contour plot of the growth principal value ratio Λ_g and the equivalent von Mises stress σ_{vM} at time step 300 s, cf. (b). For the sake of clarity the cable tie has been neglected. As an isotropic

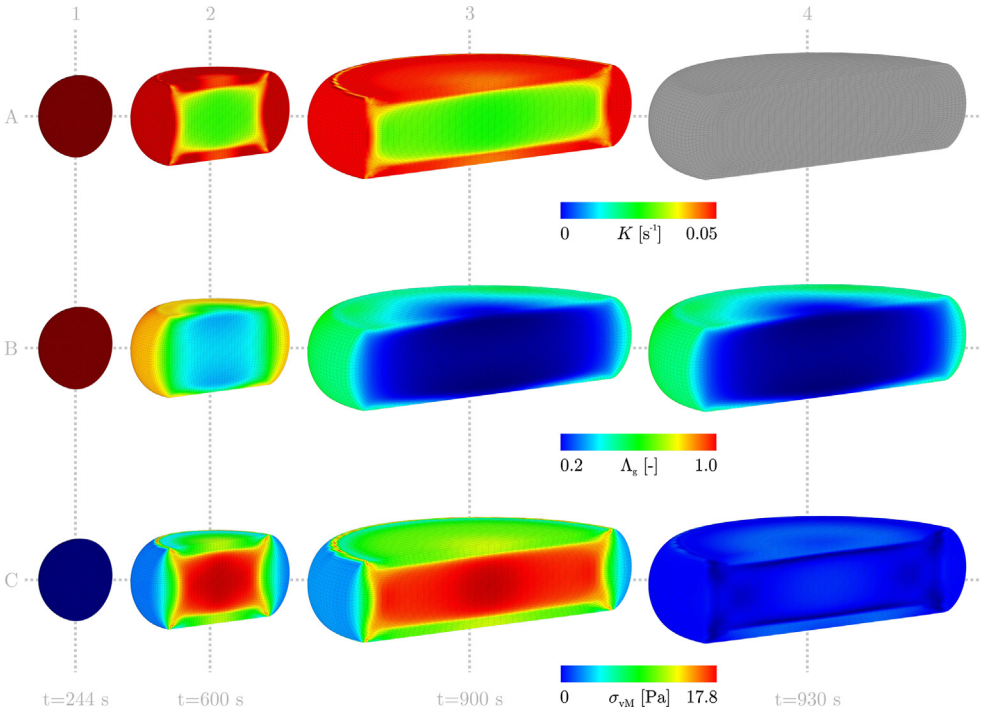

Fig. 6 – Progress of the main variables K, Λ_g, and σ_{vM} during the growth process. In order to give the reader a better view on the distribution of the different variables, only a half of the sphere is shown. Due to symmetry reasons, only a fourth of the sphere has been considered in the simulations using 29,120 hybrid linear hexahedra elements with 31,600 nodes.

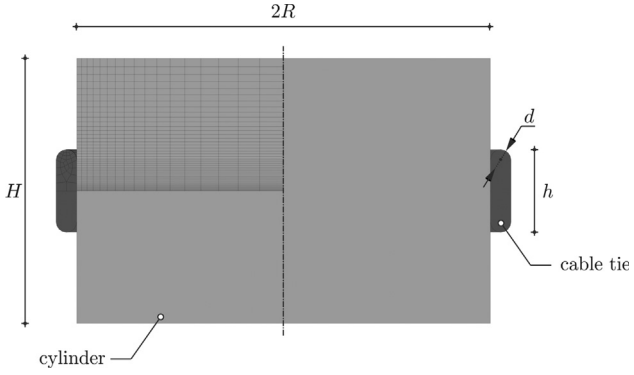

Fig. 7 – Geometry of the cylinder constrained by a cable tie. The dimensions of the system are $d/R/h/H = 0.0025/0.025/0.01/0.032$ m. For the simulation of an eighth of the system 19,200 hybrid linear hexahedra elements with 22,000 nodes have been used, cf. left upper area.

expansion is not the most favourable state for stresses, the body grows in a more relaxed direction and oozes above the cable.

Focusing first on the development of the radius *r*, it becomes obvious that a weaker cable tie leads to a higher expansion as for a stiffer one. Due to the non-linear behaviour of both, the cable tie and the growing cylinder, the increase of the radius is non-linear, too. In more detail, when focusing at time step 300 s, the stiffest material leads to increase of the radius of about 0.5%, whereby for weaker materials increases of 5% (ii) and 11% (i) can be detected. Considering the distribution of the growth principal value ratio Λ_g it stands out that the samples grow more isotropically at the top and bottom while an inhomogeneous growth can be observed in the area of the cable tie. In case of comparing example (i) with (iii) it figures out that the latter one is more subjected to an inhomogeneous growth indicated by lower values of Λ_g, especially, as expected, in the area of the cable tie. But also at the top and bottom the growth behaviour is no more purely isotropically. A similar statement is demonstrated by the stress distribution. For a stiff cable tie the maximum values are reached in the middle region of the cylinder whereas the remaining material is stress-free.

However, having in mind that high complex contact conditions have been applied in the present example the new developed modelling approach clearly demonstrated a robust implementation into the framework of the finite element method.

4. Conclusion

As demonstrated by nature, it is usual to find biological systems that grow in different ways as one would expect. Although several systems present residual stresses when boundary conditions constrain volume expansion, some bodies present fluid characteristics during growth. A well-known representative is the tree. Trees are able to grow over stones, through fences, or cracks of walls. After removing the obstacle especially older tress does not spring back pointing to the fact that at most marginal residual stresses exists, only. An other example are tumours that are (visco-plastic-)elastic bodies but behave fluid-like during growth. However, it seems obvious to describe such behaviour at continuum

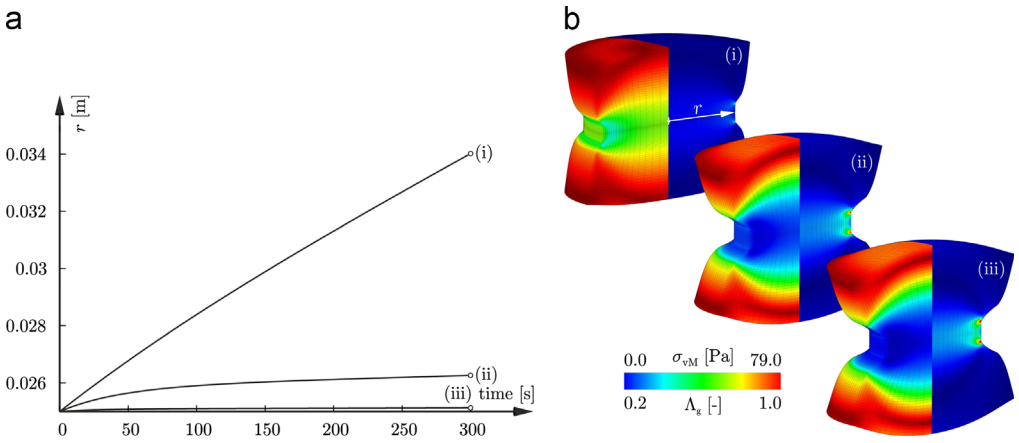

Fig. 8 – Results of the simulations: (a) development of the radius *r* in dependence on different rigidities of the cable tie (here not shown). (b) Geometry after 300 s of growth. Points (i), (ii), and (iii) correlate with those in (a) as well as to the different parameter sets, cf. Table 2. Shown are the growth principal value ratio Λ_g (*left side*) and the equivalent von Mises stress σ_{vM} (*right side*) each plotted on a quarter of the system.

level in terms of plasticity theory. But also at cellular level such behaviour can be motivated (Ambrosi and Preziosi, 2012). Thus, assuming a tumour growing against a constraint, the bonds of the cell aggregates are subjected to high tension and consequently, some of them break and form new ones. This internal reorganisation leads at macro level to stress relaxation and thus to a 'flow' of the material.

Motivated by the aforementioned arguments in the present contribution a growth concept has been developed considering inhomogeneous volume growth in biological systems. The model adapts isotropic growth of elastic bodies into a growth direction that provides a lower stress state for the same volume increment. The ability of changing growth directions is provided using a flow rule on the stress responsible for the volume preserving part of the elastic deformations. It allows for understanding and studying biological growth in cases where the grown volume behaves as an elastic body but the growth behaviour can be described using fluid-like characteristics. The model uses a predictor scheme from the supposed isotropic update to the new computed state. In fact, the presented concept covers growth characteristics of 'elastic materials growing like elastic materials' right up to 'growing fluids' and every state in between. To this end, in Section 3.1, the general performance of the growth approach is demonstrated where the two aforementioned scenarios can be seen to be border cases of the presented model. The first border case is the classical isotropic growth approach where the body grows isotropically under a given external load. When the growth process is finished and the load is removed the body forms back to a geometry which is a multiple of the initial one (Fig. 4(a)). This type of growth concept has been frequently applied to diverse issues, see e.g. recently published review by Ambrosi et al. (2011). In the second border case, the body grows like a fluid, featuring low resistance against external loads during growth. Consequently, when removing the load, the body keeps its shape (Fig. 4(d)) and shows in dependence on the used material parameters different amounts of residual stresses.

The second example deals with inhomogeneous growth due to external, rigid constraints and follows the example of Ateshian et al. (2012) where a growing sphere, representing a cell or a tumour, is placed between two constraints. This example demonstrated impressively how an initially homogeneous, isotropic material grows inhomogeneously due to external constraints. From the numerical perspective this example is challenging due to two issues: First, the sphere increases its volume 90-fold which needs a stable implementation of the model. Second, during the majority of the simulations contact needs to be considered which complicates the analysis, too. However, the outcome can be summarised as follows: In a first period the sphere grows isotropically and when it comes into contract with the constraint it develops inhomogeneously. Thereby, its shape becomes extremely deformed. The spring back of the sphere after removing the upper constraint can be controlled by the relaxation rate. Assigned to the apple example in Section 1 the analogous behaviour is realised: If the cable tie is removed, the shape of the apple is hold, mainly.

In style of the apple example, we conclude with growing cylinders, constrained by cable ties with different rigidities. In dependence on the rigidities of the cable ties the single cylinder assumes different shapes. However, the combination of a highly complex material model, an extremely inhomogeneous growth process, and the consideration of contact during the numerical simulations made this type of analyses highly challenging. To our best knowledge, there is only one contribution (Ateshian et al., 2012) dealing with those analyses. Whereas, analytical studies, e.g. on tumours in rigid cylinders, have been realised infrequently (Ambrosi and Mollica, 2002; Ambrosi and Preziosi, 2009). However, the majority of publications deals with boundary conditions due to external loads or displacements without any contact description, e.g. Göktepe et al. (2010a,b), Rausch et al. (2011), Klepach et al. (2012), and Zöllner et al. (2012), to list only a few recent published contributions.

Summarising, the presented modelling approach shows a high capability and flexibility. Anyway, despite its general good performance, when focusing on real problems as tumour growth, there are some open issues, dealing with nutrient supply/diffusion or volume restriction (the growth

process stops when a certain space is filled out), which need to be considered in future. An example of a future direction is the growth modelling of biofilms, appearing in a variety of places in daily routine (Böl et al., in press).

Acknowledgements

Partial support for this research was provided by the Deutsche Forschungsgemeinschaft (DFG) under Grant BO 3091/6-1. The authors would like to thank Dr. Alexander E. Ehret for the useful and fruitful discussions.

REFERENCES

Alastrué, V., Martínez, M.A., Doblaré, M., 2008. Modelling adaptative volumetric finite growth in patient-specific residually stressed arteries. Journal of Biomechanics 41 (8), 1773–1781.

Ambrosi, D., Mollica, F., 2002. On the mechanics of a growing tumor. International Journal of Engineering Science 40 (12), 1297–1316.

Ambrosi, D., Preziosi, L., 2009. Cell adhesion mechanisms and stress relaxation in the mechanics of tumours. Biomechanics and Modeling in Mechanobiology 8 (5), 397–413.

Ambrosi, D., Ateshian, G.A., Arruda, E.M., Cowin, S.C., Dumais, J., Goriely, A., Holzapfel, G.A., Humphrey, J.D., Kemkemer, R., Kuhl, E., Olberding, J.E., Taber, L.A., Garikipati, K., 2011. Perspectives on biological growth and remodeling. Journal of the Mechanics and Physics of Solids 59 (4), 863–883.

Ambrosi, D., Preziosi, L., Vitale, G., 2012. The interplay between stress and growth in solid tumors. Mechanics Research Communications 42 (1), 87–91.

Ateshian, G.A., Humphrey, J.D., 2012. Continuum mixture models of biological growth and remodeling: past successes and future opportunities. Annual Review of Biomedical Engineering 14 (1), 97–111.

Ateshian, G.A., Morrison III, B., Holmes, J.W., Hung, C.T., 2012. Mechanics of cell growth. Mechanics Research Communications 42 (1), 118–125.

Beck, C.B., 2010. An Introduction to Plant Structure and Development: Plant Anatomy for the Twenty-first Century, 2nd ed. Cambridge University Press, Cambridge/New York.

Ben Amar, M., Goriely, A., 2005. Growth and instability in elastic tissues. Journal of the Mechanics and Physics of Solids 53 (10), 2284–2319.

Böl, M., Ehret, A.E., Bolea Albero, A., Hellriegel, J., Krull, R. Recent advances in mechanical characterisation of biofilm and their significance for material modelling. Critical Reviews in Biotechnology 1–27, http://dx.doi.org/10.3109/07388551.2012.679250, in press.

Bolea Albero, A., Ehret, A.E., Böl, M., 2012. A continuum model for free growth in living materials. Proceedings in Applied Mathematics and Mechanics 12 (1), 123–124.

Burggren, W.W., Keller, B.B., 1997. Development of Cardiovascular Systems: Molecules to Organisms. Cambridge University Press, Cambridge, UK/New York, USA.

Cowin, S.C., 2004. Tissue growth and remodeling. Annual Review of Biomedical Engineering 6 (1), 77–107.

Dervaux, J., Ben Amar, M., 2011. Buckling condensation in constrained growth. Journal of the Mechanics and Physics of Solids 59 (3), 538–560.

Dimitriou, R., Jones, E., McGonagle, D., Giannoudis, P.V., 2011. Bone regeneration: current concepts and future directions. BMC Medicine 9 (1), 66–75.

Flory, P.J., 1961. Thermodynamics relation for high elastic materials. Transactions of the Faraday Society 57, 829–838.

Garikipati, K., Arruda, E.M., Grosh, K., Narayanan, H., Calve, S., 2004. A continuum treatment of growth in biological tissue: the coupling of mass transport and mechanics. Journal of the Mechanics and Physics of Solids 52 (7), 1595–1625.

Göktepe, S., Abilez, O.J., Kuhl, E., 2010a. A generic approach towards finite growth with examples of athlete's heart, cardiac dilation, and cardiac wall thickening. Journal of the Mechanics and Physics of Solids 58 (10), 1661–1680.

Göktepe, S., Abilez, O.J., Parker, K.K., Kuhl, E., 2010b. A multiscale model for eccentric and concentric cardiac growth through sarcomerogenesis. Journal of Theoretical Biology 265 (3), 433–442.

Helisch, A., Schaper, W., 2003. Arteriogenesis: the development and growth of collateral arteries. Microcirculation 10 (1), 83–97.

Hoger, A., 1986. On the determination of residual stress in an elastic body. Journal of Elasticity 16 (3), 303–324.

Humphrey, J.D., 2003. Review paper: continuum biomechanics of soft biological tissues. Proceedings of the Royal Society of London Series A: Mathematical and Physical Sciences 459 (2029), 3–46.

Humphrey, J.D., Rajagopal, K.R., 2002. A constrained mixture model for growth and remodeling of soft tissues. Mathematical Models and Methods in Applied Sciences 12 (3), 407–430.

Keen, R.R., Dobrin, P.B., 2000. Development of Aneurysms. Landes Bioscience, Georgetown, TX, USA.

Kim, Y., Stolarska, M.A., Othmer, H.G., 2011. The role of the microenvironment in tumor growth and invasion. Progress in Biophysics and Molecular Biology 106 (2), 353–379.

Klepach, D., Lee, L.C., Wenk, J.F., Ratcliffe, M.B., Zohdi, T.I., Navia, J.L., Kassab, G.S., Kuhl, E., Guccione, J.M., 2012. Growth and remodeling of the left ventricle: a case study of myocardial infarction and surgical ventricular restoration: recent advances in the biomechanics of growth and remodeling. Mechanics Research Communications 42, 134–141.

Koopman, R., van Loon, L.J.C., 2009. Aging exercise and muscle protein metabolism. Journal of Applied Physiology 106 (6), 2040–2048.

Kröner, E., 1959. Allgemeine Kontinuumstheorie der Versetzungen und Eigenspannungen. Archive of Rational Mechanic and Analysis 4 (1), 273–334.

Kroon, W., Delhaas, T., Arts, T., Bovendeerd, P., 2009. Computational modeling of volumetric soft tissue growth: application to the cardiac left ventricle. Biomechanics and Modeling in Mechanobiology 8 (4), 301–309.

Kuhl, E., Steinmann, P., 2003. Mass- and volume-specific views on thermodynamics for open systems. Proceedings of the Royal Society of London Series A: Mathematical and Physical Sciences 459 (2038), 2547–2568.

Lee, E.H., 1969. Elastic–plastic deformation at finite strains. Journal of Applied Mechanics 36 (1), 1–6.

Martin, P., 1997. Wound healing–aiming for perfect skin regeneration. Science 276 (5309), 75–81.

Mosler, J., Meschke, G., 2003. 3D modelling of strong discontinuities in elastoplastic solids: fixed and rotating localization formulations. International Journal for Numerical Methods in Engineering 57 (11), 1553–1576.

Moulton, D.E., Goriely, A., 2011. Circumferential buckling instability of a growing cylindrical tube. Journal of the Mechanics and Physics of Solids 59 (3), 525–537.

Rachev, A., Greenwald, S.E., 2003. Residual strains in conduit arteries. Journal of Biomechanics 36 (5), 661–670.

Rausch, M.K., Dam, A., Göktepe, S., Abilez, O.J., Kuhl, E., 2011. Computational modeling of growth: systemic and pulmonary hypertension in the heart. Biomechanics and Modeling in Mechanobiology 10 (6), 799–811.

Rodriguez, E.K., Hoger, A., McCulloch, A.D., 1994. Stress-dependent finite growth in soft elastic tissues. Journal of Biomechanics 27 (4), 455–467.

Simo, J.C., Ortiz, M., 1985. A unified approach to finite deformation elastoplastic analysis based on the use of hyperelastic constitutive equations. Computer Methods in Applied Mechanics and Engineering 49 (2), 221–245.

Skalak, R., Zargaryan, S., Jain, R.K., Netti, P.A., Hoger, A., 1996. Compatibility and the genesis of residual stress by volumetric growth. Journal of Mathematical Biology 34 (8), 889–914.

Srivastava, L.M., 2002. Plant Growth and Development: Hormones and Environment. Academic Press, Amsterdam, Netherlands/ Boston, USA.

Taber, L.A., 1995. Biomechanics of growth, remodeling, and morphogenesis. Applied Mechanics Reviews 48 (8), 487–545.

Taber, L.A., Humphrey, J.D., 2001. Stress-modulated growth, residual stress, and vascular heterogeneity. Journal of Biomechanical Engineering 123 (6), 528–535.

Tal, H., 2012. Bone Regeneration. InTech, Manhattan, USA.

Thackham, J.A., McElwain, D.L., Long, R.J., 2008. The use of hyperbaric oxygen therapy to treat chronic wounds: a review. Wound Repair and Regeneration 16 (3), 321–330.

Tomanek, R.J., Runyan, R.B., 2001. Formation of the Heart and its Regulation. Birkhäuser, Boston, USA.

Zöllner, A.M., Abilez, O.J., Böl, M., Kuhl, E., 2012. Stretching skeletal muscle: chronic muscle lengthening through sarcomerogenesis. PLoS ONE 7 (10), e45661.